Nanostructures

DOI: 10.1002/anie.200700244

One-Pot Synthesis of Manganese Oxide Nanosheets in Aqueous Solution: Chelation-Mediated Parallel Control of Reaction and Morphology**

*Yuya Oaki and Hiroaki Imai**

In biomineralization, organic molecules and polymers fulfill multiple roles in the crystallization process.[1–3] Examples of these roles include templates or scaffolds for nucleation, adsorption to growing crystals, coordination to metal ions, and control of mass transport. An exquisite association of these effects led to the emergence of biominerals with hierarchical architectures from the nanoscopic to macroscopic scale. As well as biomineralization, tailoring the interaction of organic molecules promises the realization of biomimetic crystal design in a synthetic system. The morphological changes of crystals, including their growth mechanisms, have been thoroughly investigated.[4–6] It has been reported that a strong electrostatic interaction between inorganic crystal faces and organic species resulted in morphological evolution. Along with the fundamental studies, we believe that the next challenge will be the formulation of new biomimetic routes for the preparation of hierarchical structures and functional nanomaterials. We have previously obtained hierarchically organized architectures by a concept in which organic polymers played a dual role: the strong interaction between crystal faces and polymers led to microscopic hierarchies and mass-transport controlled macroscopic shapes.[7]

On the other hand, the biomimetic synthesis and morphological control of metal-oxide nanomaterials have not been fully demonstrated in recent studies, especially in terms of two-dimensional (2D) nanostructures. An improved strategy for the simultaneous control of chemical reaction, oxidation state, crystal phase, and morphology is required for the next stage of biomimetic materials chemistry. Soft-solution processing for the synthesis of metal oxides has attracted much interest because of the relatively low temperatures.[8] However, hydrothermal and/or heat treatment and multistep processing are performed in many cases. The development of room-temperature and facile routes is also an important challenge, which can be achieved through the biomimetic pathway. We believe that the control of structure and morphology would result from a proactive approach to the coordination between metal ions and organic ligands in the precursor solutions.[9] Moreover, the coordination can be predicted from previous studies in complex and aquatic chemistry, such as the combination of Lewis acid and base.

Manganese oxides have been thoroughly investigated by several research groups because of their importance in industrial applications, such as catalysis and electrodes in lithium-ion batteries.[10–30] Among various crystal structures, much attention has been given to the birnessite type, which consists of 2D monolayers of edge-shared $\{MnO_6\}$ octahedra and alkali-metal ions and/or water molecules between the layers. Birnessite was synthesized by several methods, such as the oxidation of Mn^{2+} or $Mn(OH)_2$, the reduction of MnO_4^-, or the redox reaction of Mn^{2+}/MnO_4^- at relatively low temperature,[15–30] but morphological control on the nanoscale was not fully achieved.

Here, we report the one-pot bottom-up synthesis of manganese oxide nanosheets and their oriented thin films in aqueous solution under ambient conditions. Neither hydrothermal treatment nor special equipment was needed for this process. The addition of ethylenediaminetetraacetate (EDTA) led to the generation of birnessite nanosheets less than 10 nm in thickness. The nanosheets were deposited on substrates with a specific orientation. The synthesis and morphogenesis were controlled concurrently by the chelating agent EDTA. Chelation to the divalent manganese ion and interaction with the resultant oxide involved the formation of birnessite nanosheets in aqueous solution at room temperature, because the interaction was expected from the strength of Lewis acid and base. In earlier studies, the exfoliation of the layered structure, a typical top-down approach, resulted in the formation of manganese oxide nanosheets or nanoflakes.[31,32] However, to the best of our knowledge, neither bottom-up synthesis nor thin-film formation of nanosheets was achieved. Moreover, 2D nanostructures, including iron and cobalt oxyhydroxides, were synthesized through the same procedure. Such an approach that takes advantage of chelating agents can be generalized as a novel green route to functional nanomaterials.The reaction started upon mixing solutions containing Mn^{2+}/EDTA and NaOH (see Experimental Section). A transparent light-yellow liquid was immediately obtained, which gradually changed to a turbid dark-brown liquid within approximately 3 minutes of mixing. Precipitates were observed on the bottom of the sample bottle after about

[*] Dr. Y. Oaki, Prof. H. Imai
Department of Applied Chemistry
Faculty of Science and Technology
Keio University
3-14-1 Hiyoshi, Kohoku-ku, Yokohama 223-8522 (Japan)
Fax: (+81) 45-566-1551
E-mail: hiroaki@applc.keio.ac.jp

[**] This work was supported by the 21st Century COE program "KEIO Life Conjugated Chemistry" from the Ministry of Education, Culture, Sports, Science, and Technology, Japan, and Murata Science Foundation. Y.O. is grateful for a JSPS research fellowship for young scientists.

Supporting information for this article is available on the WWW under http://www.angewandte.org or from the author.

30 minutes, and the supernatant solution became clear and colorless after about 90 minutes. The brownish powder was precipitated at the bottom of the sample bottle. After 3 to 5 days, films were deposited on the substrates and the wall of the sample bottle.

Figure 1 a–c shows the field-emission scanning electron microscopy (FESEM) images of nanosheets less than 10 nm in thickness that were collected from the precipitates after 3 days. Interestingly, thin films of the nanosheets that were around 10 nm in thickness and 2–5 μm in width were directly deposited on the hydrophilic and hydrophobic substrates through heterogeneous nucleation after 3 to 5 days: the

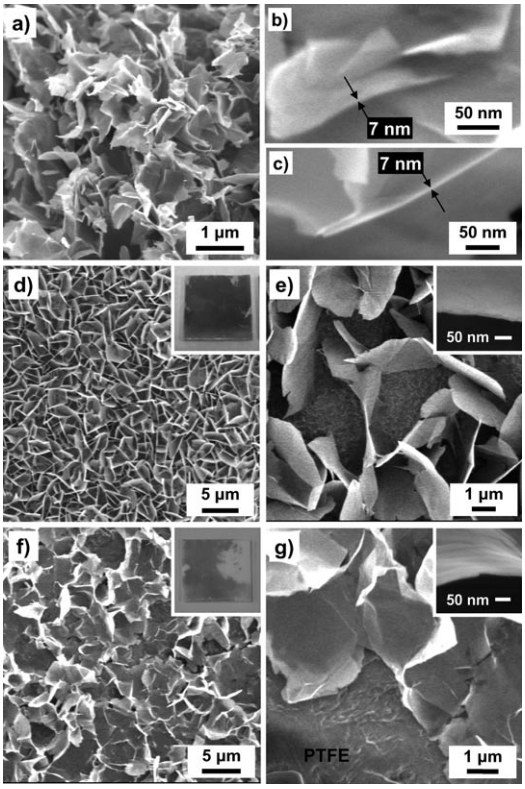

Figure 1. FESEM images of the manganese oxide nanosheets and their oriented films on the substrates. a) Precipitates; b,c) magnified images of (a); d) nanosheets arranged perpendicularly on the FTO substrate and their macroscopic appearance (inset); e) magnified images of (d); f) nanosheets deposited parallel to the PTFE substrate and their macroscopic appearance (inset); g) magnified images of (f).

nanosheets were arranged perpendicularly to the fluorine-doped tin oxide (FTO) and parallel to the polytetrafluoroethylene (PTFE) substrates (Figure 1 d–g).

According to the XRD pattern, the main product of the dried precipitates was birnessite-type manganese oxide, even though a small amount of the β-MnOOH phase was present (Figure 2 a,c).[33] The peaks assigned to birnessite were only recognized from the deposits on the wall of the sample bottle and the peak intensity ratio of (001), and the other planes were varied by the orientation of the nanosheets on the substrate (Figure 2 a,b and the Supporting Information). The selected-area electron diffraction (SAED) patterns of the

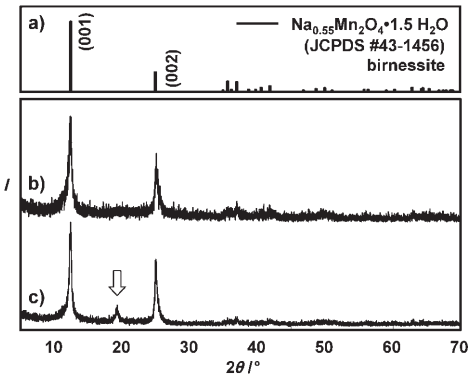

Figure 2. XRD patterns of the nanosheets. a) Peak positions of birnessite-type manganese oxide; b) nanosheets removed from the FTO substrate recorded in $2\theta/\theta$ scanning mode; c) peaks of the precipitates including birnessite and β-MnOOH (JCPDS #18-1804; indicated by arrow; see also the Supporting Information).

nanosheets showed lattice spacings of approximately 0.237 and 0.136 nm, which can be characterized as the (100) and (110) planes of birnessite, respectively (Figure 3 a). The HRTEM images corresponded to monolayers of edge-shared $\{MnO_6\}$ octahedra (Figure 3 b–d). These results indicate that the well-crystallized nanosheets were spread perpendicularly to the *c* axis of birnessite. The spotted SAED pattern suggests that the nanosheets had a single-crystalline structure (Figure 3 a). The single-crystalline nanosheets were stacked and aggregated in the *c*-axis orientation with each other, whereas the *a* and *b* axes were not aligned in several sheets. Peaks of carbon, oxygen, manganese, and sodium appeared in the energy-dispersive X-ray spectrum (EDX; see the Supporting Information). The presence of nitrogen was sometimes detected by electron energy-loss spectroscopic (EELS) analysis through the field-emission transmission electron microscopic (FETEM) observation of several nanosheets (Figure 3 e). It may be inferred that the resultant birnessite nanosheets included a small number of EDTA molecules. However, after the precipitates were washed several times with purified water, no signals resulting from the residual organic species were detected in the FTIR spectra.

The oxidation state of manganese was also estimated from the EELS analysis (Figure 3 f,g). An earlier work reported that the EELS profiles of oxygen and manganese were sensitive to the oxidation state of manganese.[34] The important parameters were the energy separation in the oxygen K edges around 540 eV and the intensity ratio of manganese L_2 and L_3 edges around 650 eV. As shown in Figure 3 f,g, the energy separation between peaks A and B in the oxygen K-edge spectrum was 11.5 eV, and the intensity ratio L_3/L_2 in the manganese spectrum was 2.23. In accordance with a previous report,[34] the data mean that the manganese species in the birnessite nanosheets adopted a state between trivalent and tetravalent. The results were quite consistent with the previous contribution regarding the oxidation states of manganese in a birnessite structure.

A colloidal liquid containing the nanosheets was readily prepared by dispersing the precipitates or thin films in water

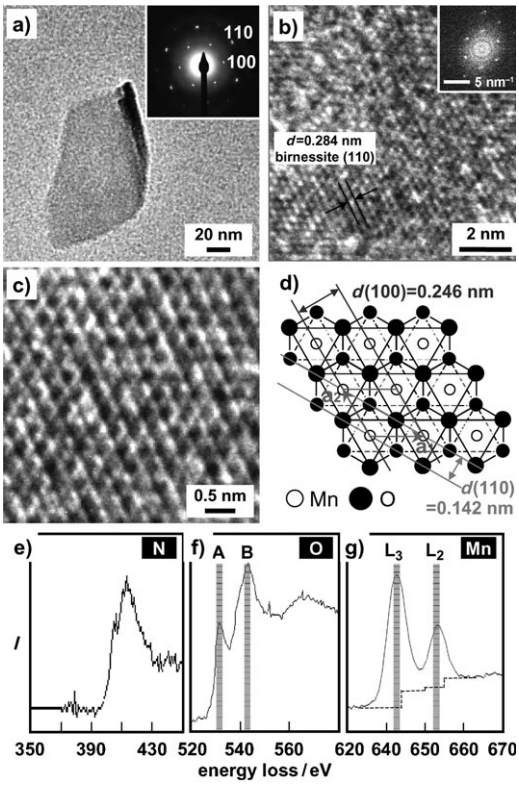

Figure 3. FETEM analysis of the nanosheets. a) Bright-field image of a single-crystalline nanosheet; inset: the spotted SAED pattern acquired around the image. b,c) HRTEM images and the fast-Fourier-transform (FFT) image (inset in b) of the nanosheets corresponding to the birnessite monolayer as represented in (d). d) Schematic model of the birnessite monolayer consisting of $\{MnO_6\}$ octahedra. e–g) EELS profiles: nitrogen K edge, which implies the presence of EDTA molecules (e), oxygen K edges (f), and manganese L_2 and L_3 edges (g). The energy separation between the two peaks in (f) and the peak intensity ratio L_3/L_2 in (g) indicate the oxidation state of manganese in the nanosheets. These EELS profiles were collected from a nanosheet and the backgrounds were subtracted.

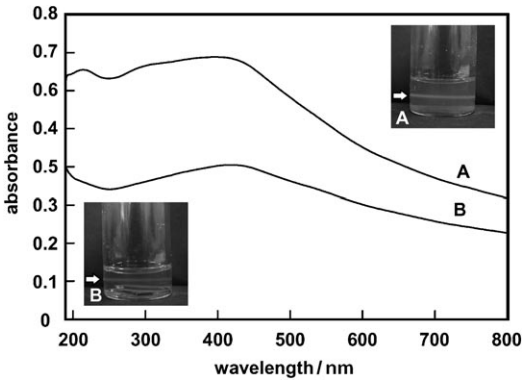

Figure 4. UV/Vis spectra of the nanosheet colloids with dispersion of the deposits on A) FTO substrate and B) precipitates.

by an ultrasonic treatment (Figure 4). The liquid dispersion is also an important precursor material for higher-ordered architectures that contain the nanosheet as a building block. The transparent brownish liquids exhibited Tyndall light scattering and a broadened absorption band centered around 420 nm in the UV/Vis spectra, even though the absorption band was not recorded in the bulk solid of birnessite by diffuse-reflectance spectroscopy. Suib et al. reported that the delamination of birnessite resulted in the appearance of a broadened absorption band within 370–450 nm.[31] As both the thickness and width of the nanosized birnessite varied depending on the type of intercalated amines, the report did not fully clarify which parameter determined the peak positions. Sasaki et al. investigated an exfoliated birnessite monolayer less than 1 nm in thickness and submicrometer in width, which showed a broadened absorption band centered around 374 nm.[32] The peak shift to approximately 410 nm in this study is concluded to be a result of slightly thicker nanosheets of about 10 nm, because the width in the submicrometric scale would not contribute to the spectroscopic changes.

In this study, we successfully achieved the one-pot synthesis of manganese oxide nanosheets and their thin films through a bottom-up approach in an aqueous solution at room temperature. To the best of our knowledge, a facile route to metal-oxide nanosheets has not been demonstrated in earlier studies. An understanding of the formation process would lead to the widespread application to other metal-oxide nanomaterials. The complexation of manganese species and EDTA molecules results in the parallel control of the reaction and morphogenesis, thus leading to birnessite nanosheets. Here, we selected a combination that considers the strength of the Lewis acid and base in aqueous solution. It is well-known that divalent manganese ions easily form $Mn(OH)_2$ and are oxidized to Mn_3O_4 by dissolved oxygen in an alkaline medium under ambient conditions.[35] When the precursor solution and sodium hydroxide were mixed in the absence of EDTA, $Mn(OH)_2$ and Mn_3O_4, which contain Mn^{II} and Mn^{III}, precipitated immediately (see the Supporting Information). On the other hand, the presence of EDTA mediated the formation of manganese oxide and oxyhydroxide with Mn^{III} and Mn^{IV} in the precipitates even before drying (Figure 2 and the Supporting Information). It is inferred that the chelation between divalent manganese ions and EDTA molecules inhibited the rapid precipitation of the hydroxide and resulted in oxidation to the trivalent and/or tetravalent states with oxygen dissolved in the precursor solutions. Thus, the formation of thin films was also achieved by heterogeneous nucleation on the substrates. The nanosheets grown parallel to the substrate contact each other and the subsequent growth proceeds in an upright direction. Thus, the frequent nucleation on the FTO substrate resulted in the preferential production of vertically standing nanosheets. On the other hand, parallel growth was mainly observed on the PTFE substrate because heterogeneous nucleation on the chemically inert PTFE surface was not so frequent as that on FTO. The mechanisms for the orientation of the nanosheets are still unclear, although a similar orientation behavior was reported in the case of layered hydroxide zinc carbonate nanosheets.[36]

The oxidized manganese species were transported with EDTA molecules to generate nanosheets consisting of edge-shared $\{MnO_6\}$ octahedra and interlayer sodium ions. Along with control of the reaction, the interaction of EDTA molecules led to the morphogenesis of birnessite nanosheets. Specific interaction on the (001) faces of birnessite would induce the formation of nanosheets with growth inhibition in the thickness direction. In this way, the chelation between inorganic and organic species can control not only the reaction, including the valence of the metal species, but also the morphology of the resultant materials. We reported that mosaic nanoflakes of manganese oxide and cobalt hydroxide were formed with incorporation of organic polymers under ambient conditions.[37] Rapid precipitation was suppressed by interaction of the polymers, as was the case with EDTA in the present study. One of the differences is that the strong adsorption of polymers resulted in growth inhibition and subsequent restarting of growth. In contrast, EDTA, a small chelating agent, preferentially promotes the reaction process rather than crystal growth. Therefore, single-crystalline nanostructures can be generated with association of EDTA, while the strong interaction of organic polymers induced nanoflakes with a mosaic interior.

We have also fabricated other 2D nanomaterials of iron and cobalt oxyhydroxides (Figure 5).[38] These trivalent metal oxyhydroxides were synthesized from divalent iron and cobalt chlorides, instead of manganese chloride, by the same procedure. The detailed structure and formation process are now under investigation.

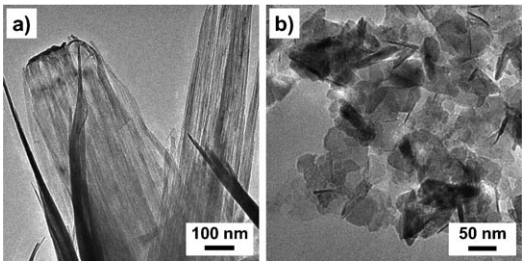

Figure 5. FETEM images of a) iron oxyhydroxide and b) cobalt oxyhydroxide nanomaterials synthesized from divalent precursors with association of EDTA.[38]

In summary, we successfully generated manganese oxide nanosheets and their oriented thin films through a bottom-up approach in an aqueous solution at room temperature. Chelation between the manganese species and EDTA molecules resulted in the formation of birnessite-type nanosheets and the deposition of thin films in a one-pot synthesis. Parallel control of the reaction and morphogenesis was realized by the EDTA molecules in the precursor solution. The synthetic method can be widely applied to other systems of metal-oxide nanostructures, because the formation of the complex between metal ions and organic additives is predictable from the strength of the Lewis acid and base. These findings strongly indicate that a proactive approach to complexation in materials chemistry realizes the design of structure, morphology, and properties of functional nanomaterials. We believe that the design of organic additives is also a significant challenge for the next step of biomimetic processing.

Experimental Section

Stock solutions containing disodium dihydrogen ethylenediaminetetraacetate (EDTA) dihydrate (20 mM; Kanto Chemical, 99.5%) were prepared in purified water at room temperature. Then, $MnCl_2{\cdot}4H_2O$ (20 mM; Kanto Chemical, 99.0%) was dissolved in the stock solution. When these materials were completely dissolved, the precursor solutions were poured into the sample bottles. The precipitates were synthesized from the precursor solution (300 mL) in polystyrene bottles (85 mm in diameter and 150 mm in height). FTO and PTFE substrates (approximately 2-cm squares) were washed with HNO_3 (1M), acetone, and purified water in a ultrasonic bath for 30 min. These substrates were immersed in the precursor solutions (25 mL) in polypropylene bottles (30 mm in diameter and 75 mm in height). Then, an equal volume of NaOH (200 mM; Junsei Chemical, 96.0%) was added to the precursor solution without stirring. The sealed sample bottles were maintained at 25°C for 3 to 5 days. The resultant precipitates were separated by centrifugation, rinsed with purified water, and dried at 25°C. The thin films were withdrawn from the solutions, rinsed with purified water, and dried at 25°C.

The morphologies were observed by FESEM (FEI Sirion microscope operated at 2.0 kV) and FETEM (FEI Tecnai F20 instrument operated at 200 kV) without any conductive treatment. The following analyses were also performed in FETEM: HRTEM, SAED, EDX (r-TEM 32), and EELS (Gatan, Imaging Filter model 607). For FETEM observations, a copper grid supported by a collodion membrane was immersed in a colloidal liquid containing the nanosheets (2 mg), which was prepared in purified water (20 mL) by using an ultrasonic bath. The resultant dispersions were also poured into a quartz cell and were used for the measurement of UV/Vis spectra (JASCO, V560). The crystal structure and orientation were characterized by XRD (Bruker, D8 Advance, $Cu_{K\alpha}$ radiation, graphite monochromator). All the samples were measured in the $2\theta/\theta$ scanning mode under ambient conditions. FTIR spectroscopy (Bio-Rad, FTS-60A) and thermogravimetry–differential thermal analysis (TG-DTA; Seiko, TG-DTA 6200) were used to detect the remaining EDTA molecules.

Received: January 18, 2007
Revised: March 21, 2007
Published online: May 22, 2007

Keywords: biomimetic synthesis · chelation · crystal growth · manganese · nanostructures

[1] a) S. Mann, *Biomineralization*, Oxford University Press, Oxford, **2001**; b) S. H. Yu, H. Cölfen, *J. Mater. Chem.* **2004**, *14*, 2124–2147, and references therein.
[2] L. Addadi, S. Weiner, *Angew. Chem.* **1992**, *104*, 159–176; *Angew. Chem. Int. Ed. Engl.* **1992**, *31*, 153–169.
[3] a) Y. Oaki, A. Kotachi, T. Miura, H. Imai, *Adv. Funct. Mater.* **2006**, *16*, 1633–1639; b) Y. Oaki, H. Imai, *Small* **2006**, *2*, 66–70.
[4] a) M. Niederberger, H. Cölfen, *Phys. Chem. Chem. Phys.* **2006**, *8*, 3271–3287; b) H. Cölfen, M. Antonietti, *Angew. Chem.* **2005**, *117*, 5714–5730; *Angew. Chem. Int. Ed.* **2005**, *44*, 5576–5591, and references therein.
[5] H. Cölfen, S. Mann, *Angew. Chem.* **2003**, *115*, 2452–2468; *Angew. Chem. Int. Ed.* **2003**, *42*, 2350–2365, and references therein.
[6] S. H. Yu, S. F. Chen, *Curr. Nanosci.* **2006**, *2*, 81–92, and references therein.
[7] a) Y. Oaki, H. Imai, *Angew. Chem.* **2005**, *117*, 6729–6733; *Angew. Chem. Int. Ed.* **2005**, *44*, 6571–6575; b) Y. Oaki, H. Imai,

Adv. Funct. Mater. **2005**, *15*, 1407 – 1414; c) Y. Oaki, H. Imai, *Chem. Commun.* **2005**, 6011 – 6013.
[8] a) M. Yoshimura, *J. Mater. Sci.* **2006**, *41*, 1299 – 1306; b) T. P. Niesen, M. R. DeGuire, *J. Electroceram.* **2001**, *6*, 169 – 207, and references therein.
[9] Y. Oaki, H. Imai, *Adv. Mater.* **2006**, *18*, 1807 – 1811.
[10] M. Hibino, H. Kawaoka, H. Zhou, I. Honma, *Electrochim. Acta* **2004**, *49*, 5209 – 5216.
[11] S. Zhu, H. Zhou, M. Hibino, I. Honma, M. Ichihara, *Adv. Funct. Mater.* **2005**, *15*, 381 – 386.
[12] N. Sakai, Y. Ebina, K. Takada, T. Sasaki, *J. Electrochem. Soc.* **2005**, *152*, E384 – E389.
[13] N. Sakai, Y. Ebina, K. Takada, T. Sasaki, *J. Phys. Chem. B* **2005**, *109*, 9651 – 9655.
[14] X.-F. Shen, Y.-S. Ding, J. Liu, J. Cai, K. Laubernds, R. P. Zerger, A. Vasiliev, M. Aindow, S. L. Suib, *Adv. Mater.* **2005**, *17*, 805 – 809.
[15] Q. Feng, H. Kanoh, K. Ooi, *J. Mater. Chem.* **1999**, *9*, 319 – 333, and references therein.
[16] J. Cai, J. Liu, S. L. Suib, *Chem. Mater.* **2002**, *14*, 2071 – 2077.
[17] S. L. Brock, M. Sanabria, S. L. Suib, V. Urban, P. Thiyagarajan, D. I. Potter, *J. Phys. Chem. B* **1999**, *103*, 7416 – 7428.
[18] J. Luo, A. Huang, S. H. Park, S. L. Suib, C.-L. O'Young, *Chem. Mater.* **1998**, *10*, 1561 – 1568.
[19] J. Luo, Q. Zhang, S. L. Suib, *Inorg. Chem.* **2000**, *39*, 741 – 747.
[20] J. Luo, S. L. Suib, *J. Phys. Chem. B* **1997**, *101*, 10403 – 10413.
[21] S. Ching, D. J. Petrovay, M. L. Jorgensen, *Inorg. Chem.* **1997**, *36*, 883 – 890.
[22] Z.-H. Liu, K. Ooi, H. Kanoh, W.-P. Tang, T. Tomita, *Langmuir* **2000**, *16*, 4154 – 4164.
[23] X. Yang, H. Kanoh, W. Tang, Z.-H. Liu, K. Ooi, *Chem. Lett.* **2001**, 612 – 613.
[24] X. Yang, Y. Makita, Z.-H. Liu, K. Sakane, K. Ooi, *Chem. Mater.* **2004**, *16*, 5581 – 5588.
[25] Q. Feng, L. Liu, K. Yanagisawa, *J. Mater. Sci.* **2000**, *35*, 1567 – 1570.
[26] Q. Feng, E.-H. Sun, K. Yanagisawa, N. Yamasaki, *J. Ceram. Soc. Jpn.* **1997**, *105*, 564 – 568.
[27] O. P. Ferreira, L. Otubo, R. Romano, O. L. Alves, *Cryst. Growth Des.* **2006**, *6*, 601 – 606.
[28] D. S. Yang, M. K. Wang, *Chem. Mater.* **2001**, *13*, 2589 – 2594.
[29] X. H. Feng, F. Liu, W. F. Tan, X. W. Liu, *Clays Clay Miner.* **2004**, *52*, 240 – 250.
[30] L. Wang, K. Takada, A. Kajiyama, M. Onoda, Y. Michiue, L. Zhang, M. Watanabe, T. Sasaki, *Chem. Mater.* **2003**, *15*, 4508 – 4514.
[31] Q. Gao, O. Giraldo, W. Tong, S. L. Suib, *Chem. Mater.* **2001**, *13*, 778 – 786.
[32] Y. Omomo, T. Sasaki, L. Wang, M. Watanabe, *J. Am. Chem. Soc.* **2003**, *125*, 3568 – 3575.
[33] The presence of β-MnOOH, as a precursor material for birnessite, was investigated in references [18] and [29].
[34] G. H. Du, Z. Y. Yuan, G. V. Tendeloo, *Appl. Phys. Lett.* **2005**, *86*, 063113.
[35] a) A. R. Nichols, J. H. Walton, *J. Am. Chem. Soc.* **1942**, *64*, 1866 – 1870; b) A. Vázquez-Olmos, R. Redón, G. Rodriguez-Gattorno, M. E. Mata-Zamora, F. Morales-Leal, A. L. Fernández-Osrio, J. M. Saniger, *J. Colloid Interface Sci.* **2005**, *291*, 175 – 180.
[36] E. Hosono, S. Fujihara, I. Honma, H. Zhou, *Adv. Mater.* **2005**, *17*, 2091 – 2094.
[37] Y. Oaki, H. Imai, *J. Mater. Chem.* **2007**, *17*, 316 – 321.
[38] According to XRD measurements, the nanosheets were assignable to α-FeOOH (goethite) and CoOOH (heterogenite). The detailed structure and formation process will be reported elsewhere.

